

TOPOLOGICAL COMPUTATION ANALYSIS OF METEOROLOGICAL TIME-SERIES DATA

HIDETOSHI MORITA*, MASARU INATSU†, AND HIROSHI KOKUBU‡

Abstract. A topological computation method (called the MGSTD method) is applied to noisy time-series data obtained from meteorological measurement. This method is based on the idea of the Morse decomposition, which is a decomposition of the dynamics into invariant sets, called the Morse sets, and their gradient-like connections. A Morse decomposition of a dissipative dynamical system can be obtained by dividing the phase space into grids and constructing a combinatorial multi-valued map over the grids [4, 6]. In the case of time-series data generated by a dynamical system, a combinatorial multi-valued map over the grids can be similarly constructed. However, time-series data obtained from real measurements (e.g., meteorological data) are often highly stochastic due to the presence of noise. A multi-valued map is then determined statistically by preferable transitions between the grids. We consider time-series data taken from the first two principal components of the pressure patterns in the troposphere and the stratosphere in the northern hemisphere, measured over 31 years, 90 days in each year \times every 6 hours per day. The application of the MGSTD method to the troposphere data yields some particular transitions between the Morse sets, corresponding to specific motions in the phase space spanned by the principal components. The motions detected by our analysis are consistent with changes between characteristic pressure patterns that have been previously recognized in meteorological studies. A similar result is also obtained with the stratosphere data.

Key words. Morse decomposition, time-series, noise, meteorology

AMS subject classifications. 37B30, 37B35, 37M10, 37N10

1. Introduction.

1.1. General background. The study of dynamics based on time-series data obtained from measurements of nonlinear phenomena has developed since the 1970s. The seminal method of delay-coordinates by Ruelle and Packard et al.[23] led to the mathematical theory of reconstructing attractors from time-series data by Aeyels [3], Takens [26], and Sauer, Yorke, and Casdagli [24]. These outcomes have been successfully applied to obtain dynamical information of a great variety of nonlinear phenomena.

The present study examines meteorological time-series data from the viewpoint of dynamical systems, and proposes a new approach for extending such time-series analysis to detect not only attractors but also unstable dynamics, by concatenating a set of time-series data derived from scattered initial conditions in the phase space of a dynamical system. The idea is based on a topological computation method to obtain a so-called the Morse decomposition, that is, a decomposition of the phase space of the dynamics into finite numbers of isolated invariant sets, called Morse sets, that are related in a gradient-like manner. This decomposition may be considered as a crude but global representation of the entire dynamics in the phase space. Recently developed computer-assisted methods for studying dynamics [1, 8, 2] enabled us to understand various aspects of the dynamics of concrete nonlinear systems. Among these methods, several authors including one of the present authors have proposed a computational approach [4, 6] for obtaining Morse decompositions together with a

* *Corresponding author*; Department of Mathematics, Kyoto University, Kyoto 606-8502, Japan (hmorita@math.kyoto-u.ac.jp)

† Faculty of Science, Hokkaido University, Sapporo, Japan (inaz@sci.hokudai.ac.jp)

‡ Department of Mathematics, Kyoto University, Kyoto 606-8502, Japan (kokubu@math.kyoto-u.ac.jp)

concise description of the dynamics of each Morse set (in terms of the Conley index) of a given dynamical system. This method was mainly developed for iterated maps with parameters, but can also be applied to ordinary differential equations [20].

The basic idea of obtaining Morse decomposition of a given dynamical system is to set a finite grid decomposition on a domain of interest in the phase space of the dynamics, and then to construct a combinatorial multi-valued map over the finite grid elements, which is a rigorous¹ outer approximation of the true time evolution of the dynamical system. Such a combinatorial multi-valued map may be represented as a finite directed graph, with nodes representing the grid elements and edges representing the time evolution from one grid element to a set of grid elements that intersect with (outer-approximation of) the true image of the given grid element. A strongly connected path component of this finite directed graph forms an isolated invariant set (or, more precisely, an isolating neighborhood whose maximal invariant subset is an isolated invariant set), and the remaining part of the directed graph becomes gradient-like, since it contains no recurrent paths.

This idea is applicable not only to the numerically computed time evolution of dynamical systems, but also to time-series data obtained from measurements of phenomena driven by unknown dynamics, if the set of time-series data is sufficiently large to capture all the essential dynamical features in the phase space. Provided this assumption holds, one may then construct a combinatorial multi-valued map from the time-series data in a similar way, and hence obtain a Morse decomposition of the underlying dynamics directly from the measurement, rather than relying on mathematical models.

1.2. Morse decomposition of the dynamics from stochastic time-series data and its application to meteorological time-series data. The dynamics of real phenomena is inevitably subjected to noise. Time-series data may thus be considered to contain some information of time evolution governed by both a deterministic dynamical system and noise. A reliable methodology is therefore essential for understanding the underlying dynamics and drawing meaningful conclusions. This may involve removing the effects of noise to obtain the deterministic contribution.

Two of the present authors and their collaborators are currently developing such a method [18], which we call the *Morse graph method for stochastic time-series data (the MGSTD method)*. Stochastic time-series in the phase space constitute an ensemble of transitions between grid elements. Extracting statistically preferred and relevant transitions yields combinatorial multi-valued map, for which Morse decomposition is performed as described above. When applied to time-series data generated from simple deterministic dynamical system models with added stochastic terms, the MGSTD method successfully reproduce the stable and unstable invariant sets, as well as their connecting orbits, of the noise-less deterministic dynamical systems. A concise demonstration is given in Subsection 2.3 below.

A natural problem of interest is to apply the MGSTD method not only to the time-series data generated from dynamical system models but also to those obtained from measurement of real phenomena. The purpose of this paper is to apply the method to time-series data obtained from meteorological measurement. The reason that, among other stochastic phenomena, we focus on the meteorological dynamics is as follows.

¹ The multi-valued maps used in this paper are constructed from time-series data generated from meteorological measurements, and therefore the results are not guaranteed to be mathematically rigorous.

First, as evidenced by the success in weather forecasting, basic physical equations governing meteorological behavior are established, such as the Navier-Stokes equation in the Earth’s rotational frame, the continuity equation for dry air and other materials, and the radiative transfer equation [9]. This enables us not only to predict a future state of meteorological variables to some extent, but also to diagnose the past and present states. Second, artificial satellites’ highly-frequent, spatially-dense, global observation has provided reliable atmospheric data with sufficient spatial and temporal resolution since the 1980s. By applying data assimilation techniques, physically consistent gridded data can be created from observation and weather forecast data [15]. Third, projecting the high-dimensional meteorological time-series data onto a limited-dimensional phase space gives globally stable orbits with a non-Gaussian probability density function [16], which implies that the motion is not completely random. In fact, although the existence of dynamically stable points was recently denied [25], the existence of preferable paths between characteristic points corresponding to atmospheric states has been indicated with the help of meteorological knowledge [17, 19]. Some deterministic aspects can therefore be expected to exist in the stochastic time-series data.

1.3. Outline of the paper. The outline of this paper is as follows. Section 2 introduces the MGSTD method. First, the mathematical theory of combinatorial Morse decomposition of dynamical systems and that of deterministic time-series data are reviewed. Next, we review the method for constructing a multi-valued map from stochastic time-series data. Examples of application to simple dynamical systems with noise are briefly presented to demonstrate the usefulness of the MGSTD method. The meteorological data, to which the MGSTD method is applied, are then presented. Section 3 reports the result of the MGSTD analysis of the datasets of the troposphere and the stratosphere. Some specific motions in the phase space are observed within highly stochastic time-series data. We examine the dependence of the results on the choice of parameter values, to see the robustness of the results. Section 4 is devoted to discussion and concluding remarks. The relevance of the observed motions to existing meteorological knowledge is discussed, and the results are shown to be consistent with, and complement to, earlier studies.

2. Method.

2.1. Morse decomposition of global dynamics from time-series data.

We here introduce the method for obtaining a Morse graph from a given time-series dataset, which is expected to represent the Morse decomposition of the dynamical system that underlies the measured time-series data. We first briefly summarize the computer-assisted method, developed in [4, 6], for obtaining a Morse decomposition of a dynamical system represented by a directed graph called a Morse graph. Section 2.1.4 applies this idea to time-series data to obtain a Morse graph of the underlying dynamical system.

2.1.1. Morse decomposition of a dynamical system. As explained above, the Morse decomposition of a dynamical systems is a decomposition of the phase space into recurrent part and gradient-like part. In this paper, we mainly consider discrete time dynamical systems, namely, an iterated map. Let X be a compact metric space and $f : X \rightarrow X$ a continuous map.

DEFINITION 2.1 (see [7]). A *Morse decomposition* of the map f is a finite collection of disjoint isolated invariant sets S_1, \dots, S_n (called *Morse sets*) with a strict partial ordering \prec on the index set $\{1, \dots, n\}$ such that, for every $x \in X \setminus \cup_{i=1}^n S_i$ and

every complete orbit $\gamma = \{x_n\}_{n \in \mathbb{Z}}$ through $x_0 = x$, i.e. $x_{n+1} = f(x_n)$ for all $n \in \mathbb{Z}$, there exist indices $i \prec j$ such that $x_n \rightarrow S_i$ and $x_{-n} \rightarrow S_j$ as $n \rightarrow +\infty$. (In this case, γ is called a *connecting orbit* from S_j to S_i .)

Here, an *isolated invariant set* $S \subset X$ of f means that it is an invariant set which has a compact neighborhood N for which S is its maximal invariant set in N and sits in its interior, namely $S \subset \text{Int } N$. The neighborhood N is called an *isolating neighborhood* of S .

Notice that Morse decomposition of a given dynamical system is not unique in general. The coarsest Morse decomposition of a map $f : X \rightarrow X$ consists of a single set S which is the maximal invariant set of f in X . If i and j are indices such that $i \prec j$ but there is no other index k such that $i \prec k \prec j$, then a coarser Morse decomposition can be created by replacing S_i and S_j with $S_i \cup S_j \cup C(i, j)$, where $C(i, j)$ denotes the union of all connecting orbits from S_j to S_i .

For two Morse decompositions $\mathcal{S} = \{S_1, \dots, S_n\}$ and $\mathcal{T} = \{T_1, \dots, T_m\}$, we say that \mathcal{S} is a refinement of \mathcal{T} , if $n \geq m$ and if there is a surjective map $\iota : \{1, \dots, n\} \rightarrow \{1, \dots, m\}$ such that $S_i \subset T_{\iota(i)}$ for any $i = 1, \dots, n$. By definition, any connecting orbit γ between S_i and S_j is also contained in T_k if $\iota(i) = \iota(j) = k$.

A Morse decomposition $\mathcal{S} = \{S_1, \dots, S_n\}$ with a partial order $i \prec j$ can be represented in terms of a directed graph $G = (V, E)$, where $V = \{S_1, \dots, S_n\}$ and $(S_j, S_i) \in E$ iff $i \prec j$. This graph is called a *Morse graph*. In order to represent the computed Morse decomposition in a compact way, it is convenient to plot a Morse graph whose edges are determined by the *transitive reduction* of the relation \prec which is a minimal relation \prec' whose transitive closure retrieves \prec . Such a representation is used below.

2.1.2. Graph representation of dynamics. To obtain a Morse decomposition of a map $f : X \rightarrow X$ with the aid of computer, we follow the idea of graph representation of the dynamics using a grid decomposition of the phase space, as given in [4]. In the case where X is a compact domain in \mathbb{R}^d , and the map $f : X \rightarrow X$ is given by a mathematical formula using functions that can be handled by numerical computation, let \mathcal{Q} be a cubical grid decomposition of \mathbb{R}^d that covers X , and we aim to compute its image $f(Q)$ for $Q \in \mathcal{Q}$ by computer. It is not in general possible to obtain the exact image by computer, and we can only expect to obtain its numerical approximation. However, the development of validated numerical computation has provided various techniques for numerically computing rigorous outer bounds. If one can compute a rigorous outer approximation $[f(Q)]$ of the image of a grid element $Q \in \mathcal{Q}$ under f (e.g., by using interval arithmetics), let $\mathcal{F}(Q)$ be the set of all grid elements in \mathcal{Q} that intersect with $[f(Q)]$, namely $\mathcal{F}(Q) = \{R \in \mathcal{Q} \mid R \cap [f(Q)] \neq \emptyset\}$. This defines a multi-valued map \mathcal{F} from \mathcal{Q} to itself. By definition, the union of all grid elements in $\mathcal{F}(Q)$ completely contains the true image $f(Q)$. In this sense, \mathcal{F} can be considered as a rigorous outer-approximation of the map $f : X \rightarrow X$. We call \mathcal{F} a *combinatorial representation* of f . Since it is a multi-valued map on \mathcal{Q} , we use the notation $\mathcal{F} : \mathcal{Q} \multimap \mathcal{Q}$ to distinguish it from a usual single-valued map.

A combinatorial representation $\mathcal{F} : \mathcal{Q} \multimap \mathcal{Q}$ of f can be equivalently represented by means of a directed graph $G = (V, E)$, where $V = \mathcal{Q}$ and $(Q, Q') \in E$ iff $Q' \in \mathcal{F}(Q)$. The analysis of G provides information on the asymptotic dynamics of f represented by \mathcal{F} . For instance, each *combinatorial invariant set* defined as a set $\mathcal{S} \subset \mathcal{Q}$ for which $\mathcal{S} \subset \mathcal{F}(\mathcal{S}) \cap \mathcal{F}^{-1}(\mathcal{S})$ represents an isolating neighborhood $|\mathcal{S}|$ with respect to f , where $|\mathcal{S}|$ stands for the geometric realization of the set \mathcal{S} of the collection of grid elements. Moreover, a *combinatorial attractor* defined as a set $\mathcal{A} \subset \mathcal{Q}$ such that $\mathcal{F}(\mathcal{A}) \subset \mathcal{A}$

represents an isolating neighborhood $|\mathcal{A}|$ whose invariant part A is stable in the sense of Conley [7]: Every forward orbit starting from a point x in some open neighborhood of A (or, more precisely, in $\text{Int}|\mathcal{A}|$) approaches A ($\text{dist}(f^n(x), A) \rightarrow 0$ as $n \rightarrow \infty$). In particular, if there exist two disjoint combinatorial attractors for \mathcal{F} , then this implies the existence of two disjoint basins of attraction for f , thus the dynamical system f is (at least) bistable.

2.1.3. Combinatorial Morse decompositions. An extensive analysis of the dynamics with its combinatorial representation can be performed by computing the *strongly connected path components*, which are defined in terms of a directed graph as the equivalent formulation of the combinatorial multi-valued map. The *strongly connected path components* of a directed graph $G = (V, E)$ are the maximal sets of vertices $C \subset V$ that satisfy the following property: for each $v, w \in C$, there exists a path from v to w with vertices in C and also a path in the opposite direction (from w to v) through C . In [14] it is shown that all the strongly connected path components of G form isolating neighborhoods for the union of all the chain recurrent sets of the dynamical system, and thus can serve as a *combinatorial Morse decomposition* $\{\mathcal{M}_i \mid i = 1, \dots, k\}$, for some $k > 0$, representing a family of isolating neighborhoods $|\mathcal{M}_i|$. The sets \mathcal{M}_i are called *combinatorial Morse sets*. A partial order \prec between the computed combinatorial Morse sets can be determined by the analysis of paths in G connecting those sets: $i \prec j$ if $i \neq j$ and if there exists a path in G from any vertex in \mathcal{M}_j to any vertex in \mathcal{M}_i . With the use of the graph G , a combinatorial Morse decomposition can be computed by algorithms introduced in [4, 5, 6]. In the following, we refer to *Morse sets* as combinatorial Morse sets $\mathcal{M}_i \in \mathcal{Q}$ and their geometrical representation $|\mathcal{M}_i| \in \mathbb{R}^d$ without distinction.

2.1.4. Combinatorial Morse decompositions from deterministic time-series data. Supposing a time-series dataset is derived from an unknown dynamical system, we seek to obtain a Morse decomposition of the underlying dynamical system. More precisely, let $f : X \rightarrow X$ be a continuous map of a compact domain $X \subset \mathbb{R}^d$, and let $\pi : X \rightarrow \mathbb{R}^m$ be an observation map. Then, for each initial point $x \in X$, we obtain a finite time-series $\{y_n\}_{n=0, \dots, N}$ given by $y_n = \pi(f^n(x))$. For a finite set $\Xi = \{x^k\}_{k \in K}$ of initial conditions in X , where K is a finite index set, and a set of natural numbers $\{N_k\}_{k \in K}$, we obtain a set D of finitely many finite time-series data as follows:

$$D = \{y_n^k = \pi(f^n(x^k)) \in \mathbb{R}^m \mid k \in K, n = 0, 1, \dots, N_k\} \quad (2.1)$$

This corresponds to the image of points $\tilde{\Xi} = \{f^n(x^k)\}_{k \in K, n=0, \dots, N_k}$ under the observation function π . For later purpose, we also define the subset

$$D' = \{y_n^k = \pi(f^n(x^k)) \in \mathbb{R}^m \mid k \in K, n = 0, 1, \dots, N_k - 1\} \quad (2.2)$$

of D .

Let \mathcal{R} be a cubical grid decomposition of a domain in \mathbb{R}^m that covers $\pi(X)$, and define $\mathcal{Y} = \{R \in \mathcal{R} \mid R \cap D \neq \emptyset\}$, and $\mathcal{Y}' = \{R \in \mathcal{R} \mid R \cap D' \neq \emptyset\}$. Then we define a combinatorial multi-valued map $\mathcal{F} : \mathcal{Y}' \multimap \mathcal{Y}$ as follows: for $R \in \mathcal{Y}$ and $R' \in \mathcal{Y}'$, we define $R \in \mathcal{F}(R')$ iff there exist $y_n^k, y_{n+1}^k \in D$ such that $y_n^k \in R'$ and $y_{n+1}^k \in R$ hold. Note that the multi-valued map \mathcal{F} should be regarded as a self-map $\mathcal{F} : \mathcal{Y} \multimap \mathcal{Y}$ as in §2.1.2. However, in practice, its domain of definition is restricted to $\mathcal{Y}' \subset \mathcal{Y}$ due to the finiteness of the time-series data.

Once \mathcal{F} is given, the same procedure as described above can be followed, yielding a finite collection $\{\mathcal{M}_p \mid p = 1, \dots, P\}$ of the strongly connected path components of the equivalent directed graph representations of \mathcal{F} , and hence the Morse graph of \mathcal{F} .

We then take a pullback of the sets $\{|\mathcal{M}_p| \mid p = 1, \dots, P\}$, namely, define $N_p = \pi^{-1}(|\mathcal{M}_p|)$. Obviously, these are disjoint compact subsets of X , since the space X is assumed to be compact. In the present situation, we assume that the unknown dynamical system is dissipative, and hence that it has a so-called global attractor, which is the maximal compact invariant set that attracts all the trajectories. It is therefore reasonable in practice to assume that X is compact, even in the case of dynamical systems driven by (dissipative) PDEs. Provided the time-series data are sufficiently abundant, one can show that these sets are indeed isolating neighborhoods and that their maximal invariant sets $M_p = \text{Inv}(N_p)$ give a Morse decomposition of the unknown dynamical system $f : X \rightarrow X$. In this paper, we do not intend to give a detailed statement of the theory nor the precise conditions for the theory to be applied, mainly because these are unverifiable in practical applications. We therefore simply note that there is some mathematical basis for this statement, even if it is not always practically meaningful for application problems [18].

2.2. Multi-valued map from stochastic time-series data. We here review a method for constructing a combinatorial multi-valued map $\mathcal{F} : \mathcal{Y}' \multimap \mathcal{Y}$ when the time-series data is noisy, as in the case of meteorological data [18].

Assume we are given a set D of m -dimensional time-series data, as in §2.1.4. A sufficiently large $\tilde{\Omega} = [-\tilde{L}, \tilde{L}]^m$ is chosen to contain D . Typically $\tilde{L} = 4$ suffices for the PCA data considered in this paper, as the PCA scores are each normalized to have zero mean and unit standard deviation. We put the grid decomposition \mathcal{R} on the domain $\tilde{\Omega}$ with grid size $h > 0$, from which the combinatorial multi-valued map is constructed. The map may depend on the setting of the grid decomposition, e.g. the size and location of the grid elements. In this paper, we only consider a square grid decomposition \mathcal{R} of the size h , and we control its location by the shift parameters $\delta_\ell \in [0, h)$ ($\ell = 1, \dots, m$). Thus, we consider the grid decomposition over the domain

$$\Omega = [-L + \delta_1, L + \delta_1] \times [-L + \delta_2, L + \delta_2] \times \cdots \times [-L + \delta_m, L + \delta_m],$$

where $L (< \tilde{L})$ is a positive integer multiple of h such that $D \subset \Omega$. Hence, a grid element in \mathcal{R} takes of the form $Q^i = [a_1^i, a_1^i + h] \times [a_2^i, a_2^i + h] \times \cdots \times [a_m^i, a_m^i + h]$ where $a_\ell^i - \delta_\ell$ is a positive integer multiple of h .

We determine a multi-valued map from the time-series as follows. We first define the initial multi-valued map $\tilde{\mathcal{F}}$ with respect to \mathcal{R} from the dataset D just as in §2.1.4, and then we modify $\tilde{\mathcal{F}}$ so as to reflect the effect of noise by taking into account of several characteristic numbers introduced below. Let ν_i be the number of data points in a grid element $Q^i \in \mathcal{R}$, namely $\nu_i = \#(Q^i \cap D)$, and $\mu_{i \rightarrow j}$ the number of transitions from Q^i to Q^j , namely $\mu_{i \rightarrow j} = \#\{(y_n^k, y_{n+1}^k) \mid y_n^k \in Q^i \cap D, y_{n+1}^k \in Q^j \cap D\}$. We then define the transition probability, or the conditional probability, from Q^i to Q^j by

$$T_{i \rightarrow j} = \mu_{i \rightarrow j} / \nu_i \quad (2.3)$$

We consider the transition between grid elements Q^i and Q^j to be determined by the transition probability, and by a parameter $\rho (\geq 1)$ indicating the degree of superiority, as follows. If $\rho < T_{i \rightarrow j} / T_{j \rightarrow i}$, then we say the transition from Q^i to Q^j is superior to the opposite transition from Q^j to Q^i , denoted by $i \rightarrow j$. Similarly, we say Q^j

to Q^i is superior to the opposite, denoted by $j \rightarrow i$, if $\rho < T_{j \rightarrow i}/T_{i \rightarrow j}$, or equivalently, $T_{i \rightarrow j}/T_{j \rightarrow i} < \rho^{-1}$. Otherwise, we say the transitions between Q^i and Q^j are comparable, denoted by $i \leftrightarrow j$. In summary,

$$i \rightarrow j \quad \text{if} \quad \rho < T_{i \rightarrow j}/T_{j \rightarrow i} \quad (2.4a)$$

$$i \leftrightarrow j \quad \text{if} \quad \rho^{-1} \leq T_{i \rightarrow j}/T_{j \rightarrow i} \leq \rho \quad (2.4b)$$

$$i \leftarrow j \quad \text{if} \quad T_{i \rightarrow j}/T_{j \rightarrow i} < \rho^{-1} \quad (2.4c)$$

Note that self transitions $i \rightarrow i$ are always taken into account unless $\mu_{i \rightarrow i} = 0$.

In addition, we avoid overestimating rare events; otherwise, for example, the transition probability for $\mu_{i \rightarrow j} = 10$ and $\nu_i = 20$ would be regarded to be equal to that for $\mu_{k \rightarrow l} = 1$ and $\nu_k = 2$, though the latter may occur just by chance. To this end, we introduce a threshold μ_* such that only the transitions $i \rightarrow j$ with $\mu_{i \rightarrow j} \geq \mu_*$ are taken into account; this threshold is also applied to self transitions. In fact, as shown below in FIG. 2.2, when μ_* is small, almost all the grids are strongly path connected, leading to a Morse set so large as to cover all the relevant domain in the phase space; with increasing μ_* , such a Morse set is divided into several Morse sets, some of which are robustly seen for various choices of the other parameters; when μ_* is too large, even relevant transitions are removed, leaving only independent Morse sets with no transitions between them.

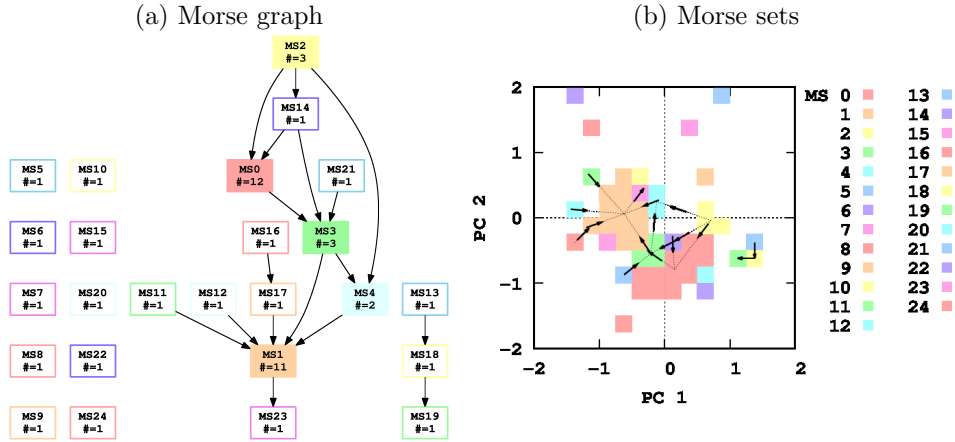


FIG. 2.1. (a) Sample Morse graph and (b) the corresponding Morse sets for the troposphere, with $h = 0.25$, $\rho = 1.1$, $(\delta_1, \delta_2) = (0, 0)$, and $\mu_* = 8$. Morse sets are denoted by MS_i ($i = 0, 1, 2, \dots$), and ordered according to size, which also determines the color coding of the Morse sets. Note that isolated Morse sets of unit size may be spurious resulting from slow dynamics. The color coding is the same in (a) and (b). In (a), the Morse sets of size two or more are filled with color. In (b), the arrows and dotted lines, connecting the barycenters of Morse sets, represent the gradient-like connections in the Morse graph in (a). See also the MGSTD algorithm below.

We thus define the multi-valued map \mathcal{F} by $Q^j \in \mathcal{F}(Q^i)$, if $Q^j \in \tilde{\mathcal{F}}(Q^i)$, either $i \rightarrow j$ or $i \leftrightarrow j$, and $\mu_{i \rightarrow j} \geq \mu_*$ are all satisfied. FIG. 2.1 is a sample Morse graph and the corresponding Morse sets, in the case of $m = 2$, obtained from the meteorological time-series data explained below in §2.4. Notice that the Morse graph in FIG. 2.1(a) can be recovered using the arrows in FIG. 2.1(b), which also exhibit the location of the corresponding Morse sets in the phase space. We call such a presentation of the Morse graph the *phase space presentation of the Morse graph*, and we adopt it in the following.

We thus have $4+m$ control parameters: m, h, ρ, μ_* , and $\delta_1, \delta_2, \dots, \delta_m$ for defining the multi-valued map \mathcal{F} . Among them, we set the dimension of the ‘phase space’ $m = 2$ throughout the paper, following earlier studies [16, 17, 13, 12].

Two issues must be addressed to extract information about the ‘deterministic’ transitions arising from the unknown underlying dynamics and distinguished from the stochastic time-series data: (A) how to select parameters of computation, and (B) how to exhibit the aspects of transitions from the results of computation. Our approach, explained below, is called the *Morse graph method for stochastic time-series data* (abbrev. as the *MGSTD method*).

With regard to the issue (A), after fixing the number of principal components $m = 2$, we vary the other $m + 3 = 5$ parameters, namely the grid size h , the degree of superiority ρ for determining the direction of transition between grid elements, the threshold μ_* for the number of transitions between grid elements, and δ_1, δ_2 ($0 \leq \delta_\ell < h, \ell = 1, 2$), the position of the center of the grid.

An essential parameter is μ_* . Since the original data is highly stochastic, a single large Morse set may be obtained as a result of stochastic recurrence in the data, if μ_* is inappropriately set (See FIG. 2.2). For each pair of grid elements, the transitions occurring less frequently than μ_* times are discarded, considered to result from stochasticity. As μ_* is increased, fewer pairs of grid elements display transitions, meaning a decrease in the chance of recurrence. Upon reaching some value of μ_* , a single large Morse set splits into several smaller Morse sets of comparable size.

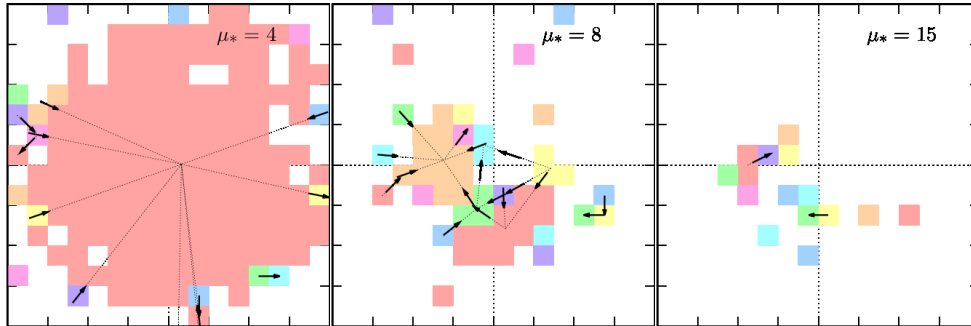


FIG. 2.2. Example of showing the splitting of Morse sets with increasing μ_* in the troposphere, with $h = 0.25$, $\rho = 1.1$, and $(\delta_1, \delta_2) = (0, 0)$. The abscissa and ordinate are PC1 and PC2, respectively, in all panels.

It is therefore reasonable to set the smallest value of μ_* for which the large single Morse set splits into several Morse sets of comparable size. The value may be estimated by the ratio of the sizes of the two largest Morse sets. More specifically, we select μ_*° as

$$\mu_*^\circ = \min \left\{ \mu_* \mid \frac{\#(\text{MS}_{\text{first}})}{\#(\text{MS}_{\text{second}})} < A \right\}$$

where $\#(\text{MS}_{\text{first}}[\text{resp. second}])$ is the size (i.e. the number of grid elements) of the first and second Morse sets (ordered according to size) for a given μ_* , and A is a value suitably chosen from the data.

The above ratio is computed by varying μ_* for fixed values of ρ, h , and δ_ℓ . A sharp drop is observed at some values of μ_* (FIG. 2.3). Using the above criterion, the first value of μ_* after the sharp drop is selected, giving $\mu_*^\circ = 8$ for the troposphere

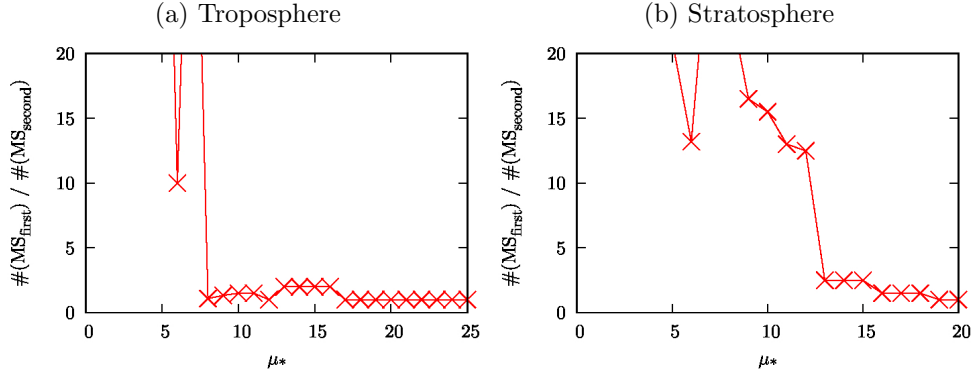


FIG. 2.3. Dependence on μ_* of the ratio $\#(\text{MS}_{\text{first}})/\#(\text{MS}_{\text{second}})$ for (a) the troposphere and (b) the stratosphere; $h = 0.25$, $\rho = 1.1$, $(\delta_1, \delta_2) = (0, 0)$.

and 13 for the stratosphere. In both cases, any value of A between 3 and 9 gives the same values for μ_*° . We have therefore chosen $A = 5$ for the computations throughout the paper.

All the above computations were done with $\rho = 1.1$ and $h = 0.25$; see below for details of how to set these values.

With regard to the issue (B), we introduce the idea of a ‘vector field’ to display temporal transitions between Morse sets, by the following algorithm.

MGSTD algorithm:

- Step 0: Fix $\mu_* = \mu_*^\circ$, and vary δ_1, δ_2 each from 0 to h with some increment (e.g., 0.01).
- Step 1: Compute the Morse graph and its Morse sets.
- Step 2: For each gradient-like connection between Morse sets in the Morse graph, namely for each arrow from one Morse set MS_i to one of its descendent Morse sets, say MS_j , compute the vector v_{ij} that is parallel to the vector $p_i - p_j$, where p_k ($k = i, j$) is the barycenter of $|\text{MS}_k|$, and such that its length $|v_{ij}| = (\#(\text{MS}_i) + \#(\text{MS}_j))/2$. The center of v_{ij} is placed at the $\#(\text{MS}_i) : \#(\text{MS}_j)$ interpolation point q_{ij} of p_i and p_j . We thus obtain the distribution of vectors v_{ij} for all the arrows in the Morse graph.
- Step 3: For a choice of δ_1, δ_2 , and a grid element R , take an ‘average’ of the vectors v_{ij} whose centers belong to R , by dividing their sum by their number and placing it at the center of R . This vector is denoted by $v_R(\delta_1, \delta_2)$. This gives a distribution of the vectors over the grid \mathcal{R} , for δ_1, δ_2 .
- Step 4: Take an ‘average’ of the distribution of the vectors by varying δ_1, δ_2 as follows. For each grid element Q in the canonical grid decomposition \mathcal{Q} with $\delta_1 = 0, \delta_2 = 0$, compute the average $w(Q)$ of all the vectors $v_R(\delta_1, \delta_2)$ whose centers belong to Q . Place the vector $w(Q)$ at the center of the grid element Q .

We thus obtain the ‘vector field’ $\{w(Q) \mid Q \in \mathcal{Q}\}$ over the canonical grid decomposition \mathcal{Q} , which we call the *MGSTD vector field*. In §2.3, we shall apply the MGSTD method to some mathematical models and compute the Morse graphs as well as the MGSTD vector fields.

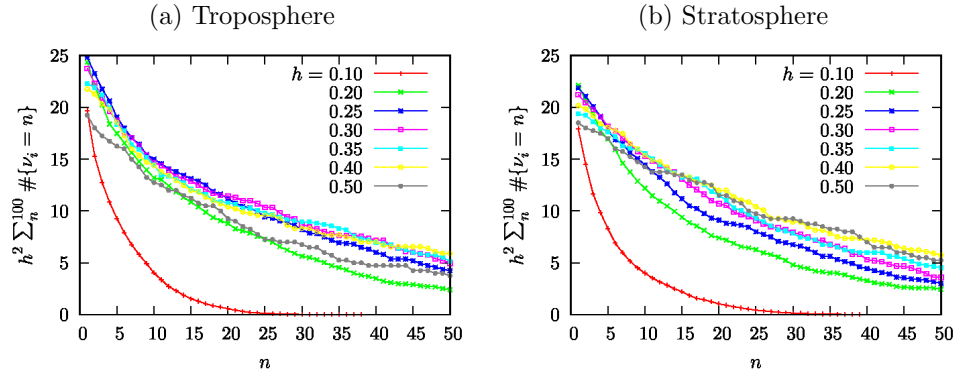


FIG. 2.4. The relative portion of the grid elements of the size h in the domain of the PC1-PC2 plane that carry n or more data points, for (a) the troposphere and (b) the stratosphere.

The grid size h suitable for extracting the important aspects of dynamics hidden in the time-series data is determined as follows. Since the unity of PC1 and PC2 is their standard deviation in which most of the data points are, each unit square of the PC1-PC2 plane should be divided at least several times, e.g., into 3^2 , 4^2 , or 5^2 pieces, by choosing small values of h , e.g., $h = 1/3, 1/4$ or $1/5$, respectively. Most of the grid elements, on the other hand, should contain sufficiently many number of data points, so that the transition probability among grid elements is relevant. Smaller value of h implies, however, smaller number of data points in a grid element. A suitable lower bound for h that meets the above two requirements is determined by considering $h^2 \sum_n^{100} \#\{\nu_i = n\}$, i.e., the relative portion of the grid elements of size h in the domain of the PC1-PC2 plane that carry n or more data points. Here, the number $n = 100$ in the summation is practically considered as infinity. The dependence of this quantity on n is shown in FIG. 2.4 for varying h . By regarding between 10 and 20 data points as sufficient in a grid element, the relative portion is maximal at around $h = 0.25$ for the troposphere, and at around $h = 0.3$ for the stratosphere. This meets the above requirements, namely the unit square of the PC1-PC2 plane is divided into 4^2 and 3^2 grid elements for the troposphere and the stratosphere, respectively, and the relative ratio of the grid elements that contain between 10 and 20 data points is maximal. In order to see the robustness of the computation results to the value of h , we also vary h in the range of $0.2 \leq h \leq 0.3$ for the troposphere, and of $0.25 \leq h \leq 0.35$ for the stratosphere.

The remaining parameter to be determined is ρ . The value should not be very different from the unity, otherwise unnecessarily many pairs of grid elements would be regarded to have bidirectional transitions, hence preventing the detection of meaningful dynamics in the data. We therefore adopt $\rho = 1.1, 1.3$, and 1.5 for the computations.

2.3. Application to mathematical models. We here briefly demonstrate the application of the MGSTD method to simple dynamical systems with noise. Further details of the analysis will appear elsewhere [18].

We consider the one-dimensional stochastic differential equation,

$$dx_t = x_t(1 - x_t^2)dt + \sigma dB_t, \quad (2.5)$$

where B_t denotes a standard one-dimensional Brownian motion [21]. Without noise ($\sigma = 0$), there exist two stable fixed points at $x = \pm 1$ and one unstable fixed point at $x = 0$. We set $\sigma = \sqrt{0.2}$ in the following.

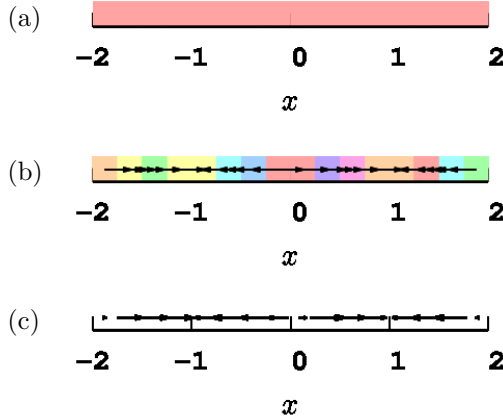


FIG. 2.5. (a) Morse set for (2.5) with the dataset D_1^{1D} without parameter setting other than $h = 0.25$, (b) Morse sets and the phase space presentation of the Morse graph for (2.5) with the dataset D_1^{1D} with $h = 0.25$, $\rho = 1.1$, $\delta_1 = 0$, and $\mu_*^\circ = 2$, (c) MGSTD vector field $\{w(Q)\}$ for (2.5) with the dataset D_2^{1D} with $h = 0.25$, $\rho = 1.1$, and $\mu_*^\circ = 1$ (the average is 1).

We first consider the case where sufficiently many number of data are given; we take 1000000 initial points uniformly randomly distributed over the interval $[-2, 2]$, and, for each initial point, we make one step time evolution by integrating (2.5) over the time interval $[0, \Delta t]$ with a time step of $\Delta t = 0.1$. We performed the integration using the stochastic Runge-Kutta method [10] with a time increment 0.001. Thus we obtain the dataset of the form (2.1),

$$D_1^{1D} = \{\xi_n^k = x_{n\Delta t}^k \mid k = 1, \dots, 1000000, n = 0, 1\}.$$

When the multi-valued map is determined without using the parameter setting given in §2.2, the resulting Morse graph becomes as shown in FIG. 2.5(a), with one large Morse set covering the relevant region of the one-dimensional phase space. When the multi-valued map is determined by applying the MGSTD method with the above criterion of parameter setting, the Morse graph changes to that shown in FIG. 2.5(b), with two Morse sets at around $x = 1$ (orange) and $x = -1$ (yellow), corresponding to the sink vertices of the Morse graph, and a Morse set at around $x = 0$ (red), corresponding to the source vertex of the Morse graph.

We next consider the case where insufficiently many number of data are given, just like the case of the meteorological data in §2.4; we take 30 initial points uniformly randomly distributed over the interval $[-2, 2]$, and make 399 steps time evolution by integrating (2.5) over the time interval $[0, 10 - \Delta t]$ with a time step of $\Delta t = 0.025$. These numbers are almost as many in number as the number of the meteorological data sets that we are going to analyze. The integration scheme is the same as the above. The dataset thus obtained is,

$$\tilde{D}_2^{1D} = \{x_t^a \in \mathbb{R} \mid a = 1, \dots, 30, t = n\Delta t, n = 0, 1, \dots, 399\}.$$

We consider this as the dataset of the form (2.1),

$$D_2^{1D} = \{\xi_n^k \in \mathbb{R} \mid k \in K, n = 0, 1, \dots, 99\}$$

with the index set $K = \{(a, c) \mid a = 1, \dots, 30, c = 0, 1, 2, 3\}$, by $\xi_n^k = x_t^a$ with $t = 0.1n + 0.025c$. Due to the shortage of the number of data points, the Morse graph

in this case depends strongly on the choice of the origin of grid δ_1 . Even in such a case, however, the MGSTD vector field $\{w(Q)\}$ shows a similar structure of the aspects of transitions between Morse sets as shown in FIG. 2.5(c), namely there are accumulation of arrows around $x = 1$ and -1 , and separation at around $x = 0$. We can therefore say that the MGSTD method qualitatively reproduces the deterministic nature of (2.5) without noise.

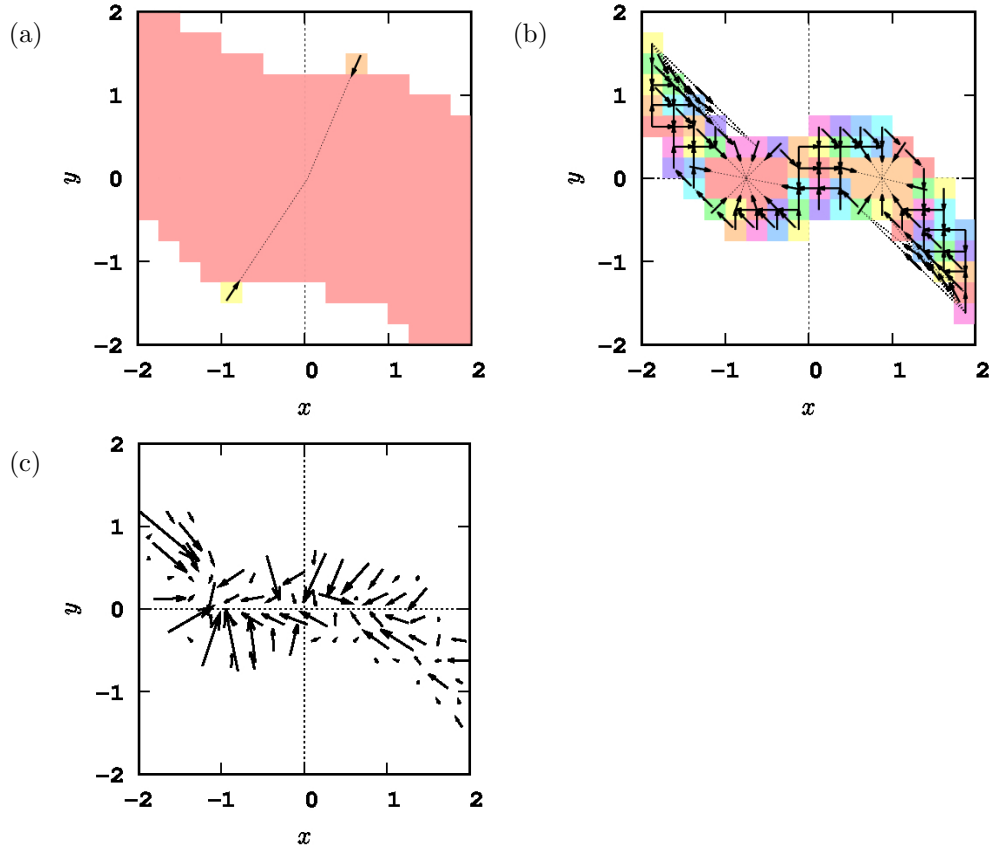


FIG. 2.6. (a) Morse sets and the phase space presentation of the Morse graph for (2.6) with the dataset D_1^{2D} without parameter setting other than $h = 0.25$, (b) Morse sets and the phase space presentation of the Morse graph for (2.6) with the dataset D_1^{2D} with $h = 0.25$, $\rho = 1.1$, $(\delta_1, \delta_2) = (0, 0)$, and $\mu_*^\circ = 461$, (c) MGSTD vector field $\{w(Q)\}$ for (2.6) with the dataset D_2^{2D} with $h = 0.25$, $\rho = 1.1$, and $\mu_*^\circ = 3$ (the average is 2.20).

We also perform a similar analysis for the two-dimensional stochastic differential equation,

$$\begin{cases} dx_t = y_t dt + \sigma dB_t^x, \\ dy_t = [-4y_t + x_t(1 - x_t^2)]dt + \sigma dB_t^y, \end{cases} \quad (2.6)$$

where B_t^x and B_t^y denote two independent standard Brownian motions. Without noise ($\sigma = 0$), there exist two sinks at $(\pm 1, 0)$ and one saddle at $(0, 0)$. We set $\sigma = \sqrt{0.08}$ in the following.

We similarly consider two datasets of the form (2.1),

$$D_1^{2D} = \{(\xi_n^k, \eta_n^k) = (x_{n\Delta t}^k, y_{n\Delta t}^k) \in \mathbb{R}^2 \mid k = 1, \dots, 1000000, n = 0, 1\},$$

and

$$D_2^{2D} = \{(\xi_n^k, \eta_n^k) \in \mathbb{R}^2 \mid k \in K, n = 0, 1, \dots, 99\}$$

with the index set $K = \{(a, c) \mid a = 1, \dots, 30, c = 0, 1, 2, 3\}$, by $(\xi_n^k, \eta_n^k) = (x_t^a, y_t^a)$ with $t = 0.1n + 0.025c$. Here, for D_1^{2D} , we take 1000000 initial points that are uniformly randomly distributed over the square $[-2, 2] \times [-2, 2]$, and, for each initial point, we make one step time evolution by integrating (2.5) over the time interval $[0, \Delta t]$ with a time step of $\Delta t = 0.1$, whereas for D_2^{2D} , we take 30 initial points uniformly randomly distributed over the square $[-2, 2] \times [-2, 2]$, and make 399 steps time evolution by integrating (2.6) over the time interval $[0, 10 - \Delta t]$ with a time step of $\Delta t = 0.025$.

When the multi-valued map is determined from the dataset D_1^{2D} without using the parameter setting given in §2.2, the resulting Morse graph becomes as shown in FIG. 2.6(a), while it is determined by applying the MGSTD method with the above criterion of parameter setting, the Morse graph changes to that shown in FIG. 2.6(b), with two relatively large Morse sets at around $(1, 0)$ (orange) and $(-1, 0)$ (red), corresponding to the sink equilibria of the deterministic ODE (without noise), and a Morse set at around $(0, 0)$, corresponding to the saddle equilibrium. The result for the dataset D_2^{2D} is given in FIG. 2.6(c). In this case, similarly to the one-dimensional case, the result of Morse graphs depend on the choice of (δ_1, δ_2) , but the MGSTD vector field given in FIG. 2.6(c) qualitatively reproduces the flow of (2.6) without noise.

2.4. Meteorological data. We here explain the meteorological data to which the MGSTD method is applied. We obtained a set of time-sequence vectors based on a re-analysis dataset, in which many types of satellite observation data and special sounding observation are assimilated with a weather forecast model and a three-dimensional variational analysis method, named JRA25/JCDAS archived by the Japan Meteorological Agency [22]. The dataset represents synoptic to global meteorological phenomena on a scale greater than several hundred kilometers with 1.25 degrees by 1.25 degrees mesh spacing, and covers a recent period with a 6-hour interval since many meteorological satellites were launched. The analysis period is restricted to three winter months, December, January, and February, from 1979/80 to 2010/11, and then we used 32 (year) data segments of 90 (day) \times 4 (data per day) length in time. The analysis domain is the whole domain north from 20°N, with the grid-points being 288 in longitude and 57 in latitude. After subtracting the trivial seasonal cycle from the data, the low-pass filter extracting variations with a period longer than 10 days was taken for the geopotential height anomaly at a specific isobaric surface of 500 hPa for the tropospheric case and 10 hPa for the stratospheric case. The isobaric geopotential height is conventionally used by meteorologists for the identification of upper-air low or high pressure systems. The principal component analysis applied to the low-frequency variability (LFV) data eventually provided a set of time-series vectors with its component being 288×57 : only the first and second modes that we used explain approximately 25 % of the LFV variance for the tropospheric case and 65 % of the LFV variance for the stratospheric case, respectively. The phase space is then spanned by two orthonormal bases of these first and second PC modes, just as [13, 12].

The dataset thus obtained is, for both the troposphere and the stratosphere,

$$\tilde{D}^L = \{(\tilde{y}_1(a, b, c), \tilde{y}_2(a, b, c)) \in \mathbb{R}^2 \mid a = 1, \dots, 32, b = 1, \dots, 90, c = 0, 6, 12, 18\}$$

where L indicates either the troposphere or the stratosphere, $\tilde{y}_\ell(a, b, c)$ ($\ell = 1, 2$) is the score of the PC_ℓ , and a , b , and c denote year, day, and o'clock, respectively. We consider this as the dataset of the form (2.1),

$$D^L = \{(y_1^k(n), y_2^k(n)) \in \mathbb{R}^2 \mid k \in K, n = 1, \dots, 90\}$$

with the index set $K = \{(a, c) \mid a = 1, \dots, 32, c = 0, 6, 12, 18\}$, by $y_\ell^k(n) = \tilde{y}_\ell(a, n, c)$; notice that $(y_1^k(n), y_2^k(n))$ corresponds to y_n^k in (2.1). Accordingly, the subset of the form (2.2) is,

$$D'^L = \{(y_1^k(n), y_2^k(n)) \in \mathbb{R}^2 \mid k \in K, n = 1, \dots, 89\}$$

The MGSTD method is hence applied to this dataset D^L .

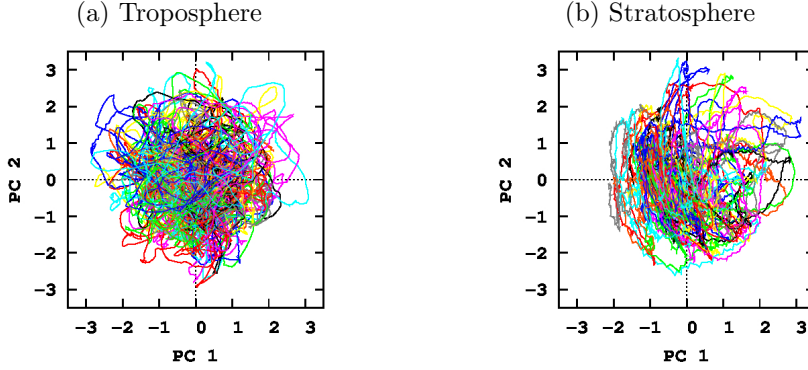


FIG. 2.7. Trajectories projected onto the $PC1$ - $PC2$ plane for (a) the troposphere and (b) the stratosphere. Different colors denote different years.

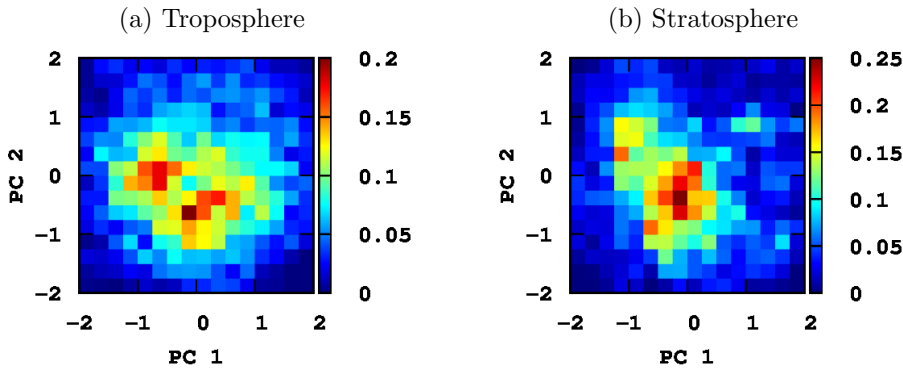


FIG. 2.8. Probability density functions of $PC1$ and $PC2$ for (a) the troposphere and (b) the stratosphere. The grid size $h = 0.25$.

The trajectories of thus obtained time-series data of the PC scores for the troposphere and the stratosphere are projected onto the $PC1$ - 2 plane in FIG. 2.7, which

show highly stochastic dynamics. The probability density functions of PC1 and PC2, shown in FIG. 2.8, display skewed, non-Gaussian forms. This is related to the existence of several known, persistent, characteristic patterns of the pressure field detected as local departure from two-dimensional Gaussian PDF in the phase space. For the troposphere (FIG. 2.8-(a)), in particular, those at around $(\text{PC1}, \text{PC2}) = (0, -1)$, $(1, 0)$, $(1, 1)$, and $(-1, 0)$ are called ZNAO, PNA, BNAO, and RNA, respectively. (Note that the PC2 is upside down compared with [16].)

These spatial patterns are dominant week-to-month variability and have a great impact to weather systems in the Northern Hemisphere. For example, a pair of ZNAO and BNAO are long recognized as a see-saw pattern of Azores high and Icelandic low pressures in the North Atlantic, which is usually called the North Atlantic Oscillation (NAO) (originally [27] but see [11] for the overview of NAO studies). The positive phase of NAO, say ZNAO, shifts the jet stream, the storm-track, and precipitation poleward, while the negative phase of NAO shifts them equatorward. On the other hand, a pair of PNA and RNA has been recognized as a see-saw pattern across the Pacific to North America, which is usually called the Pacific-North American (PNA) pattern. A positive phase with intensifying the Aleutian low and a negative phase respectively corresponds to PNA and RNA in this paper. The typical Rossby-wave train propagates from the equatorial North Pacific to the south-eastern US via Alaska [28]. A transition between ZNAO and RNA and another transition cycling PNA, BNAO, RNA, ZNAO, and backing to PNA were statistically discussed in [17].

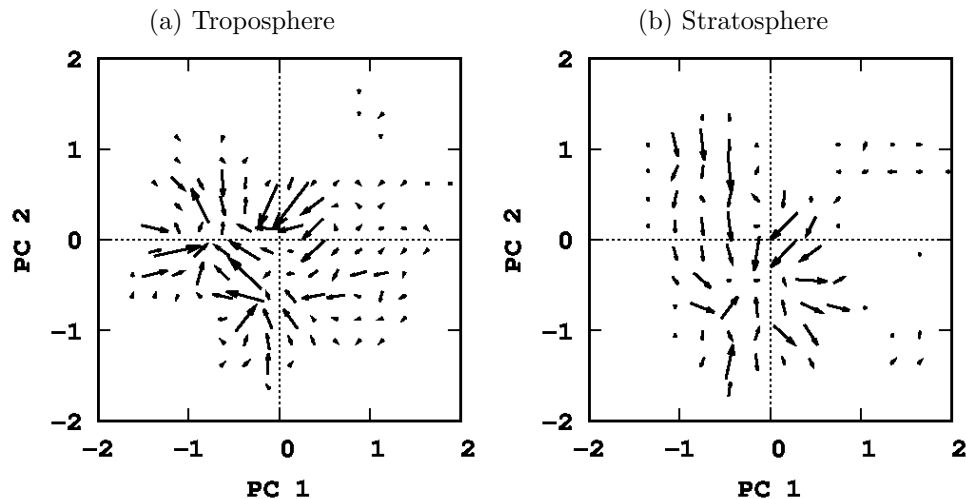


FIG. 3.1. MGSTD vector fields for (a) the troposphere with the dataset D^{tropo} , and $h = 0.25$, $\rho = 1.1$, $\mu_*^{\circ} = 8$ (the average 7.76), and (b) the stratosphere with the dataset D^{strato} , and $h = 0.3$, $\rho = 1.1$, $\mu_*^{\circ} = 15$ (the average 14.51).

3. Result. To determine the parameters for use in the analysis, as discussed in §2.2, we first chose $m = 2$, and studied the datasets D^{tropo} for the troposphere and D^{strato} for the stratosphere. We chose $h = 0.25$ from D^{tropo} and $h = 0.3$ from D^{strato} , according to the criterion from FIG. 2.4 and in the accompanying explanation.

Fixing $\rho = 1.1$, we computed μ_*° by varying δ_1, δ_2 . Its average values over δ_1, δ_2 are $\mu_*^{\circ} = 7.76$ for the troposphere and $\mu_*^{\circ} = 14.51$ for the stratosphere. Since μ_* must be an integer by definition, we chose $\mu_*^{\circ} = 8$ for the troposphere and $\mu_*^{\circ} = 15$ for the

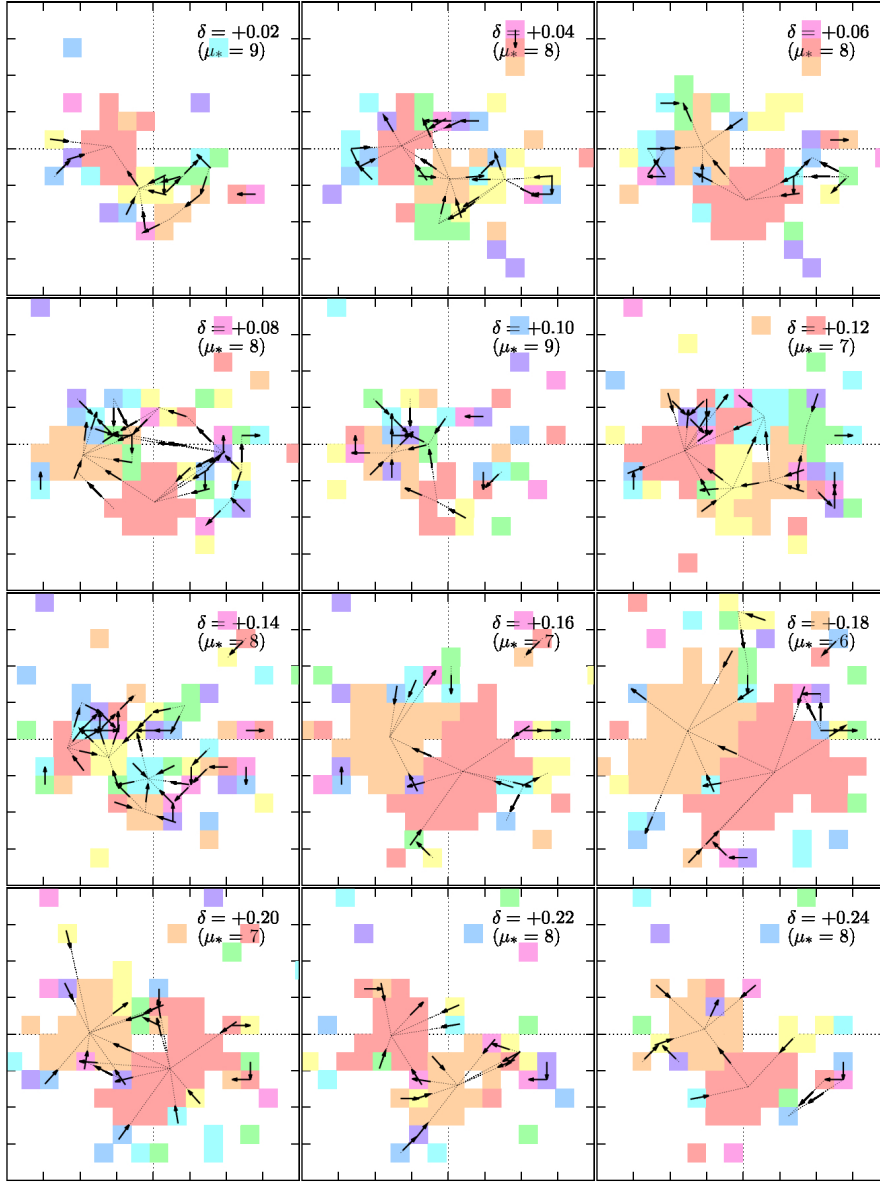


FIG. 3.2. Morse sets and the phase space presentation of the Morse graphs for D^{tropo} with $(\delta_1, \delta_2) = \delta(1, 0)$ for varying $\delta = 0.02$ to 0.24 (see FIG. 2.1 for $\delta = 0$); $h = 0.25$, $\rho = 1.1$. The abscissa and ordinate are PC1 and PC2, respectively, in all panels.

stratosphere.

For the troposphere, the MGSTD vector field for D^{tropo} with $h = 0.25$, $\rho = 1.1$, and $\mu_*^o = 8$ is shown in FIG. 3.1(a). We observe leftward and down-leftward motions in the fourth quadrant, and up-leftward motion in the third quadrant. We also observe a motion from the first to the second quadrant through a vicinity of the origin.

The phase space presentations of the Morse graphs for various choices of δ_1, δ_2 are shown in FIG. 3.2, together with the corresponding μ_*^o . In most cases, the motions

observed in the MGSTD vector field are consistent with transitions between Morse sets. In particular, the up-leftward motion in the third quadrant seems to correspond to the transition between the two largest Morse sets, from the one at around $(0, -1)$ to that at around $(-1, 0)$. Moreover, in some cases, a Morse set around $(1, 0)$ seems to be involved in the leftward and down-leftward motions in the fourth quadrant, especially as a (successive) transition to the Morse set at around $(0, -1)$, and in the motion from the first to the second quadrant through a vicinity of the origin.

These dominant motions are commonly observed over a finite range of h and ρ , as shown in FIG. 3.4.

For the stratosphere, the MGSTD vector field for D^{strato} with $h = 0.3$, $\rho = 1.1$, and $\mu_*^\circ = 15$ is shown in FIG. 3.1(b). We observe motions to a sink-like location at around $(-0.25, -0.25)$, and a downward motion in the second and third quadrants. We also observe a leftward motion in the first quadrant, though it is less prominent than the previous one.

The phase space presentations of the Morse graphs for various choices of δ_1, δ_2 are shown in FIG. 3.3, together with the corresponding μ_*° . In most cases, the motions observed in the MGSTD vector field are again consistent with transitions between Morse sets. In particular, the sink seems to correspond to a relatively large Morse set at around $(-0.25, -0.25)$ that tends to attract transitions inward. Moreover, the downward motion in the second and third quadrants seems to correspond to successive transitions between Morse sets downward in the second and third quadrants. In addition, in some cases, the leftward motion in the first quadrant seems to correspond to the leftward or left-and-downward transitions between Morse sets in the first quadrant.

These dominant motions are again commonly observed over a finite range of h and ρ , as shown in FIG. 3.5.

4. Discussion and concluding remarks. For the troposphere, we have observed two dominant motions. One is left-downward in the fourth quadrant, and the other is left-upward in the third quadrant, by detecting the clockwise circular dynamics from a Morse set around $(1, 0)$ to one around $(0, -1)$ and then to another around $(-1, 0)$. Noting that the choice of signs of PC scores is arbitrary, a comparison of the probability density function in FIG. 2.8(a) with that reported previously in [16] indicates that these motions correspond to the transitions from PNA to ZNAO and that from ZNAO to RNA, respectively. Luo et al. [19] investigated a characteristic weather pattern in a transition path from ZNAO to BNAO and another transition path from BNAO and ZNAO in the Atlantic Ocean. The former transition is through the Scandinavia blocking high with a negative PC1 projection, and the latter is through the Atlantic ridge with a positive PC1 projection [29]. This is consistent with our analysis.

For the stratosphere, we have observed a dominant motion downward from the second to the third quadrant. This is associated with a wave-energy charge by the vertical propagation of Rossby waves with their zonal wavenumber one. We have also observed another dominant sink-like location at around $(-0.25, -0.25)$. This corresponds to the resetting of the characteristic pattern, as PC1 and PC2 both become near zero. The small difference results from the skewness of the data set distribution. There is also a less prominent motion directed leftward in the first quadrant. This may be related to the final stage of an event called the stratospheric sudden warming. These results are also consistent with earlier studies [12].

For the troposphere, the transitions between weather regimes which previous studies detected have relied on meteorological knowledge. An advantage of our pro-

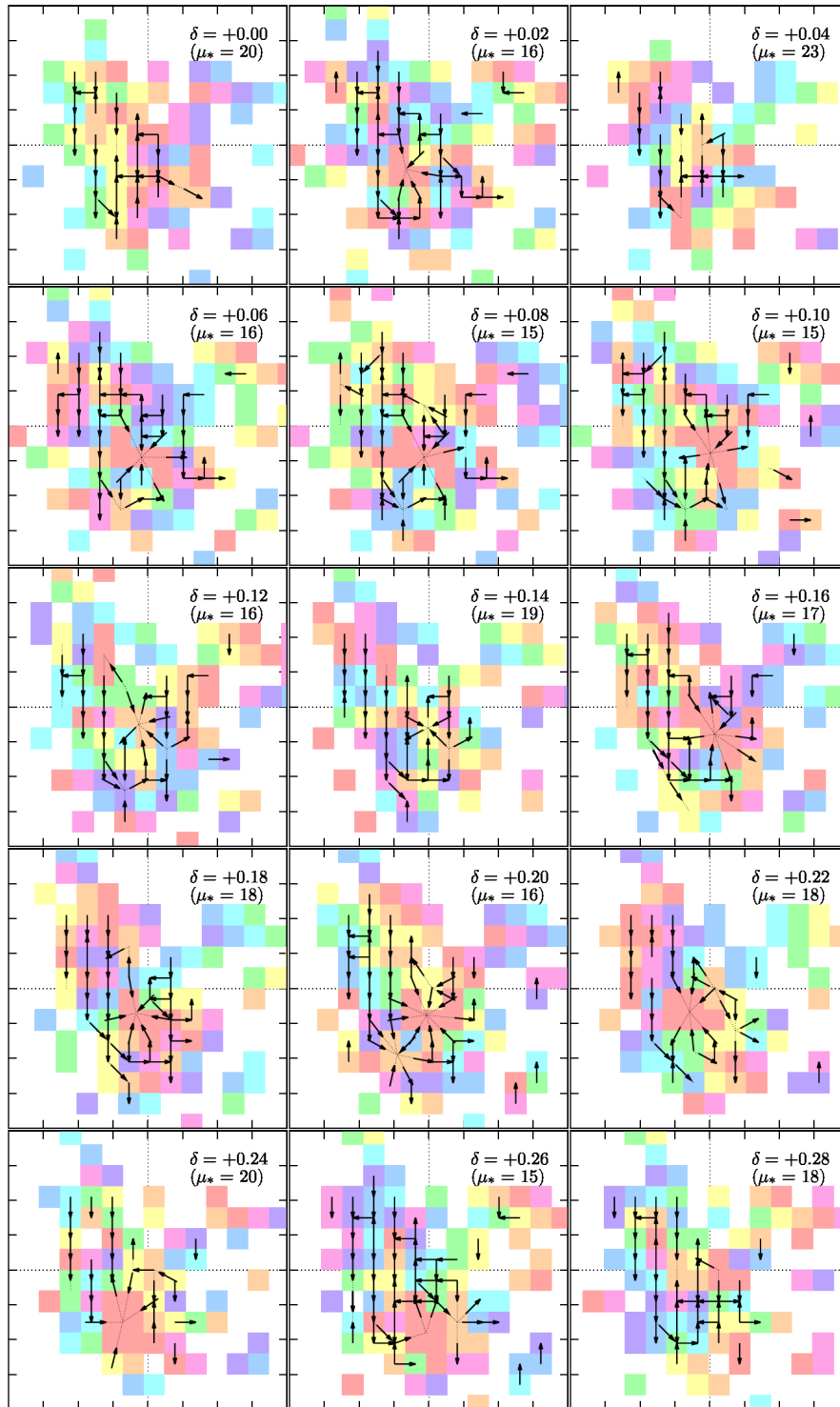


FIG. 3.3. Morse sets and the phase space presentation of the Morse graphs for D^{strato} with $(\delta_1, \delta_2) = \delta(1, 0)$ for varying $\delta = 0.0$ to 0.28 ; $h = 0.3$, $\rho = 1.1$. The abscissa and ordinate are $PC1$ and $PC2$, respectively, in all panels.

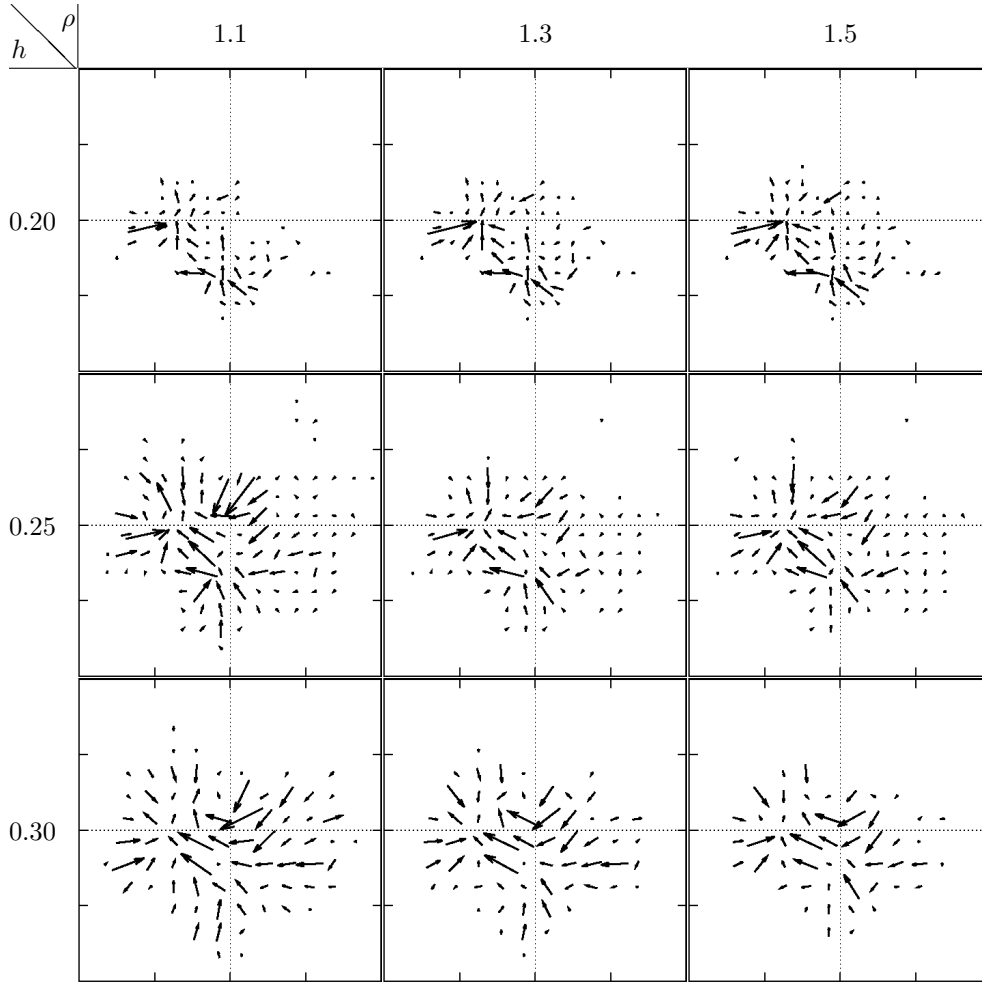


FIG. 3.4. MGSTD vector fields for the troposphere with D^{tropo} for varying h and ρ . The values of μ_2^* (resp. the average) are, from left to right, top to bottom, 6 (5.29), 6 (5.36), 6 (5.42), 8 (7.76), 9 (8.05), 9(8.23), 11 (10.52), 12 (11.50), 13 (12.17). The abscissa and ordinate are PC1 and PC2, respectively, in all panels.

posed method is that such patterns can be identified without any meteorological foresight. For the stratosphere, the stratospheric sudden warming and the subsequent polar-vortex amplification were well known and explained with atmospheric dynamics. However, the method presented in this paper can identify this transition only from the time-series data.

The results demonstrate the efficacy of the proposed method not only for time-series derived from model dynamical systems but also for that from real measurements. Furthermore, this kind of automatic analysis techniques, including machine learning, could be helpful in scientific fields with a massive amount of data like meteorology.

Acknowledgement

The authors are grateful to Masaki Nomura for helping to calculate the Morse graphs. This work was supported by JST CREST, and by JSPS KAKENHI Grant Numbers

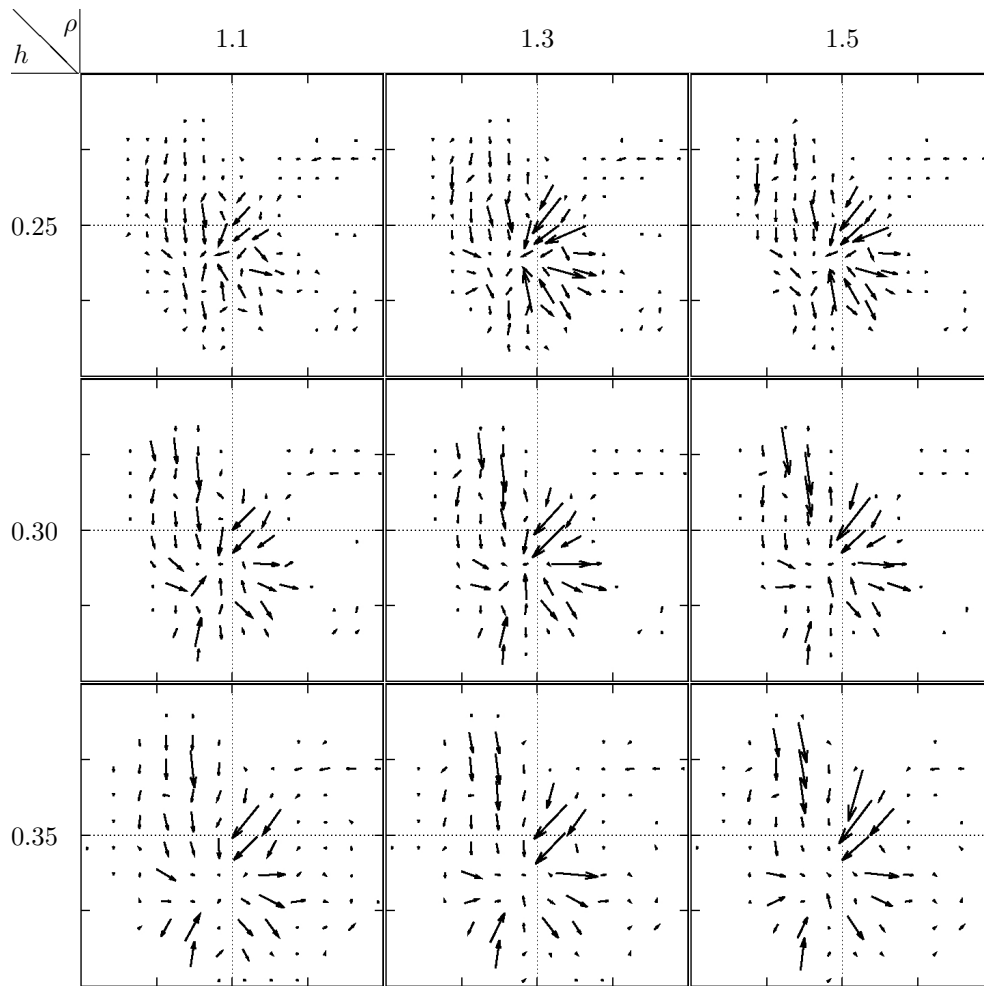


FIG. 3.5. MGSTD vector field for the stratosphere with D^{strato} for varying h and ρ . The values of μ_*^* (resp. the average) are, from left to right, top to bottom, 13 (12.06), 13 (12.94), 14 (13.60), 15 (14.51), 16 (15.93), 17 (16.51), 16 (15.90), 18 (17.80), 19 (18.82). The abscissa and ordinate are PC1 and PC2, respectively, in all panels.

JP25287029, JP26310208, and JP18H03671. MI was partly supported by JSPS KAKENHI Grant Numbers JP25610028, JP26310201, and JP18K03734.

REFERENCES

- [1] *Auto* — software for continuation and bifurcation problems in ordinary differential equations. <http://indy.cs.concordia.ca/auto/>.
- [2] *Computer assisted proofs in dynamics*. <http://capd.wsb-nlu.edu.pl/>.
- [3] DIRK AEYELS, *Generic observability of differentiable systems*, SIAM Journal on Control and Optimization, 19 (1981), pp. 595–603.
- [4] Z. ARAI, W. KALIES, H. KOKUBU, K. MISCHAIKOW, H. OKA, AND P. PILARCZYK, *A Database Schema for the Analysis of Global Dynamics of Multiparameter Systems*, SIAM Journal on Applied Dynamical Systems, 8 (2009), pp. 757–789.
- [5] HYUNJU BAN AND WILLIAM D KALIES, *A computational approach to Conley’s decomposition theorem*, Journal of Computational and Nonlinear Dynamics, 1 (2006), pp. 312–319.

- [6] J. BUSH, M. GAMEIRO, S. HARKER, H. KOKUBU, K. MISCHAIKOW, I. OBAYASHI, AND P. PILARCZYK, *Combinatorial-topological framework for the analysis of global dynamics*, Chaos, 22 (2012), p. 047508.
- [7] CHARLES C. CONLEY, *Isolated invariant sets and the Morse index*, no. 38 in CBMS Regional Conference Series in Mathematics, American Mathematical Society, Providence, R. I., 1978.
- [8] MICHAEL DELLNITZ, GARY FROYLAND, AND OLIVER JUNGE, *The algorithms behind gaio – set oriented numerical methods for dynamical systems*, in Ergodic theory, analysis, and efficient simulation of dynamical systems, Berndt Fiedler, ed., Springer, 2001, pp. 145–174.
- [9] JAMES R. HOLTON AND GREGORY J. HAKIM, *An introduction to dynamic meteorology*, Academic Press, 2012.
- [10] REBECCA L. HONEYCURTT, *Stochastic Runge-Kutta algorithms, I: White noise*, Physical Review A, 45 (1992), pp. 600–603.
- [11] J. W. HURRELL, Y. KUSHNIR, G. OTTERSEN, AND M. VISBECK, *An overview of the North Atlantic Oscillation. The North Atlantic Oscillation: Climatic Significance and Environmental Impact*, Geophys. Monogr., 134 (2003), Amer. Geophys. Union, pp. 1–36.
- [12] M. INATSU, N. NAKANO, S. KUSUOKA, AND H. MUKOUGAWA, *Predictability of wintertime stratospheric circulation examined by non-stationary fluctuation dissipation relation*, Journal of Atmospheric Sciences, 72 (2015), pp. 774–786.
- [13] M. INATSU, N. NAKANO, AND H. MUKOUGAWA, *Dynamics and practical predictability of extratropical wintertime low-frequency variability in a low-dimensional system*, Journal of Atmospheric Sciences, 70 (2013), pp. 939–952.
- [14] WILLIAM D. KALIES, KONSTANTIN MISCHAIKOW, AND ROBERT CAM VANDERVORST, *An algorithmic approach to chain recurrence*, Foundations of Computational Mathematics, 5 (2005), pp. 409–449.
- [15] EUGENIA KALNEY, *Atmospheric modeling, data assimilation and predictability*, Cambridge University Press, 2002.
- [16] M. KIMOTO AND M. GHIL, *Multiple Flow Regimes in the Northern Hemisphere Winter. Part I: Methodology and Hemispheric Regimes.*, Journal of Atmospheric Sciences, 50 (1993), pp. 2625–2644.
- [17] ———, *Multiple Flow Regimes in the Northern Hemisphere Winter. Part II: Sectorial Regimes and Preferred Transitions.*, Journal of Atmospheric Sciences, 50 (1993), pp. 2645–2673.
- [18] HIROSHI KOKUBU, HIDETOSHI MORITA, MASAKI NOMURA, AND IPPEI OBAYASHI, *Conley-Morse graph analysis of time series*. in preparation.
- [19] D. LUO, J. CHA, AND S.B. FELDSTEIN, *Weather Regime Transitions and the Interannual Variability of the North Atlantic Oscillation. Part II: Dynamical Processes*. J. Atmos. Sci., 69 (2012), pp. 2347–2363.
- [20] T. MIYAJI, P. PILARCZYK, M. GAMEIRO, H. KOKUBU, K. MISCHAIKOW, *A study of rigorous ODE integrators for multi-scale set-oriented computations*, Applied Numerical Mathematics, 107 (2016), pp. 34–47.
- [21] BERNT ØKSENDAL, *Stochastic differential equations*, Springer, sixth ed., 2013.
- [22] KAZUTOSHI ONOGI, JUNICHI TSUTSUI, HIROSHI KOIDE, MASAMI SAKAMOTO, SHINYA KOBAYASHI, HIROAKI HATSUSHIKA, TAKANORI MATSUMOTO, NOBUO YAMAZAKI, HIROTAKA KAMAHORI, KIYOTOSHI TAKAHASHI, SHINJI KADOKURA, KOJI WADA, KOJI KATO, RYO OYAMA, TOMOAKI OSE, NOBUTAKA MANNOJI, AND RYUSUKE TAIRA, *The jra-25 reanalysis*, Journal of the Meteorological Society of Japan. Ser. II, 85 (2007), pp. 369–432.
- [23] N. H. PACKARD, J. P. CRUTCHFIELD, J. D. FARMER, AND R. S. SHAW, *Geometry from a time series*, Phys. Rev. Lett., 45 (1980), pp. 712–716.
- [24] T. SAUER, J. A. YORKE, AND M. CASDAGLI, *Embedology*, Journal of Statistical Physics, 65 (1991), pp. 579–616.
- [25] D. B. STEPHENSON, A. HANNACHI, AND A. O’NEILL, *On the existence of multiple climate regimes*, Quarterly Journal of the Royal Meteorological Society, 130 (2004), pp. 583–605.
- [26] FLORIS TAKENS, *Detecting strange attractors in turbulence*, in Dynamical systems and turbulence, vol. 898 of Lecture Notes in Mathematics, Springer, 1981, pp. 366–381.
- [27] G. T. WALKER, *Correlation in seasonal variation of weather. IX. A further study of world weather*, Mem. Ind. Meteor. Dept., 24, (1924), pp. 275–333.
- [28] J. M. WALLACE AND D. S. GUTZLER, *Teleconnections in the geopotential height field during the Northern Hemisphere winter*, Mon. Wea. Rev., 109 (1981), pp. 784–812.
- [29] T. M. WOOLINGS, J. G. PINTO, AND J. A. SANTOS, *Dynamical evolution of North Atlantic ridges and poleward jet stream displacements*. J. Atmos. Sci., 68 (2011), pp. 954–963.